Lean Flame Stabilization with Nanosecond Plasma Discharges in a Gas Turbine Model Combustor

Victorien Blanchard, Frédéric Roqué, Philippe Scouflaire, Christophe O Laux, Sebastien Ducruix

LEAN FLAME STABILIZATION WITH NANOSECOND PLASMA DISCHARGES IN A GAS TURBINE MODEL COMBUSTOR

Blanchard, Victorien P.
Laboratoire EM2C, CNRS, CentraleSupélec, Université Paris-Saclay
3, rue Joliot-Curie
91190 Gif-sur-Yvette, France
victorien.blanchard@centralesupelec.fr

Roqué, Frédéric
Laboratoire EM2C, CNRS, CentraleSupélec, Université Paris-Saclay
3, rue Joliot-Curie
91190 Gif-sur-Yvette, France

Scouflaire, Philippe
Laboratoire EM2C, CNRS, CentraleSupélec, Université Paris-Saclay
3, rue Joliot-Curie
91190 Gif-sur-Yvette, France

Laux, Christophe O.
Laboratoire EM2C, CNRS, CentraleSupélec, Université Paris-Saclay
3, rue Joliot-Curie
91190 Gif-sur-Yvette, France

Ducruix, Sébastien
Laboratoire EM2C, CNRS, CentraleSupélec, Université Paris-Saclay
3, rue Joliot-Curie
91190 Gif-sur-Yvette, France

ABSTRACT

This paper presents an experimental study of lean flames stabilization with nanosecond repetitively pulsed discharges. The two-stage, swirled-stabilized, multipoint injector BIMER operates at atmospheric pressure with methane-air mixtures in the present study. It is representative in its design of a realistic lean premixed prevaporized injector of gas turbine engines operated at a lab-scale level. The lean blow-off extension with plasma is characterized. The combustion efficiency and the pollutant emissions are quantified near blow-off with and without plasma for 50-kW flames. We show that it is possible to stabilize lean flames down to an equivalence ratio of 0.3, with less than 5 ppm of NO_X emitted, thanks to NRP discharges with an electric power that represents less than 0.25% of the flame thermal power. This study also clearly shows that it is necessary to account for the plasma system integration at the early stage of the combustor design to fully benefit from the plasma stabilizing effects on the flame.

Keywords: plasma-assisted combustion, NRP discharges, gas turbine, lean flames, pollutant emissions, NO_X reduction, combustion efficiency

1. INTRODUCTION

The reduction of NO_X emissions is an essential requirement for the development of future gas turbines and jet engines. For example, the European Commission targets a reduction of 90% of aircraft NO_X emissions by 2050 relative to the 2000 level (FlightPath 2050 [1]). Lean premixed combustion is a promising approach that requires new injector technologies. Various geometries and injection strategies have been proposed by engine manufacturers and academic communities [2]. For instance, injection of fuel in a crossflow of air can efficiently mix fuel and air [3]–[5]. To control combustion instabilities, staged injection of fuel and air has also been investigated [6]–[8]. This enables flexibility and modulation of the local equivalence ratios and of the flow conditions to ensure flame holding. Despite the progress made to control lean premixed combustion through injector design, these flames are still prone to instability and extinction [2].

Nonequilibrium plasmas are known to enhance the combustion and improve the performance of lean flames [9]–

[11]. In particular, Nanosecond Repetitively Pulsed (NRP) discharges [12] are of prime interest because of the high reduced electric field triggering thermochemical effects beneficial to combustion stabilization at a low power budget [13], [14].

Much work has been done on the stabilization of lean flames with NRP discharges. For instance, the lean blow-off (LBO) extension of propane-air flames was demonstrated in Ref. [15] and the mitigation of thermo-acoustic instabilities was studied in Refs. [16]–[18]. A few works report experiments closer to practical applications such as the LBO extension in a swirl-stabilized burner using liquid dodecane in [19], or gaseous methane at high-pressure [20]. In addition, the LBO was dramatically extended with NRP discharges in a gas turbine model combustor in Ref. [21].

The combustion efficiency and the pollutant emissions of lean flames stabilized by NRP discharges were characterized in several studies [17], [22]–[26]. For the conditions of these studies, the NO_X emissions increased when the NRP discharges were applied. The CO emissions did not increase in Refs. [23], [24]. Choe & Sun [25] measured a reduction of CO emissions when NRP discharges were applied, due to an improved combustion efficiency. Moreover it was shown in Ref. [22]–[24] that the level of NO_X emitted by plasma-assisted flames was lower than the level of NO_X emitted in air only with the same NRP discharges. This trend, however, was not confirmed by Choe & Sun.

Several parameters of the NRP discharges can influence NO_X emissions. Lacoste *et al.* [24], Kim *et al.* [17], and Xiong *et al.* [26] measured a linear increase of NO_X emissions with the discharge repetition frequency. Choe & Sun did not observe a significant effect of the repetition frequency, but the range of repetition frequencies tested was narrow. NO_X emissions also increase with the peak voltage and, at constant air flow rate, with the plasma electric power [17], [25], [26]. Lacoste *et al.* varied the air flow rate and showed that NO_X emissions linearly increase with the plasma power per unit mass of air injected in the combustor. In contrast, according to Choe & Sun, NO_X emissions divided by the plasma power are governed mainly by the pulse peak voltage rather than the pulse repetition frequency due to the plasma chemistry which is more sensitive to the reduced electric field. The sensitivity of NO_X emissions to the different parameters discussed above depends on the range of variation of these parameters, on the type of burner, and on the location of the NRP discharges. Additional studies are thus needed to draw general conclusions.

One of the goals of plasma-assisted combustion is to stabilize lean flames with low NO_X emissions. However, when applying NRP discharges in premixed methane-air flames, Refs. [23] and [24] showed that the level of NO_X remained constant for equivalence ratios from 1 to 0.7. In Ref. [25], the authors observed a similar plateauing value for equivalence ratios between 0.75 and 0.55 and a lower plateauing value for equivalence ratios from 0.4 to 0.2. This suggests that it is possible to reduce the NO_X emissions of plasma-assisted flames at very low equivalence ratios. However, the combustor in Ref. [25] was operated at a flame thermal power less than 5 kW. The objective of the present work is to assess the ability of NRP discharges to stabilize lean flames in a combustor that is more representative of a gas turbine engine at a much higher power and to characterize the pollutant emissions and the combustion efficiency.

2. EXPERIMENTAL SETUP AND DIAGNOSTICS

2.1 BIMER-PAC experimental setup

The BIMER-PAC burner, shown in Figure 1, consists of a combustion chamber with a square cross-section of 15-cm width and 50-cm length. It is dedicated to plasma-assisted combustion studies and has been duplicated from an existing facility [27]–[29]. In this study, the burner is operated with gaseous methane at atmospheric pressure. The chamber backplane, as well as its upper and lower walls, are water-cooled to ensure thermal equilibrium when operating in steady state. The side walls are made of silica to provide optical access and continuous monitoring of the flame. Two small silica windows facing each other are inserted in the upper and lower walls close to the injector for laser diagnostics. K-type thermocouples are mounted in the water-cooling circuit of each wall to monitor the temperature in order to determine the heat flux extracted at the walls. A thermocouple is inserted in the injector downstream of the multipoint stage swirling vane to detect flame flashback. To monitor the wall surface temperature, two thermocouples are integrated in the lower wall via blind holes. The thermocouples are recessed 1 mm from the wall inner surface to prevent them from receiving radiation from the flame. They are located along the centerline of the wall at 25 cm and 42 cm from the chamber backplane, respectively.

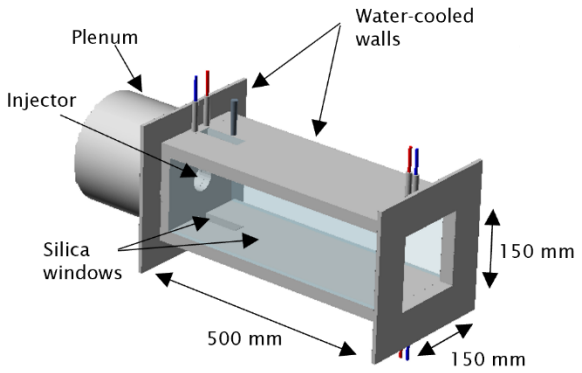

FIGURE 1 COMBUSTOR OF THE BIMER-PAC FACILITY, ADAPTED FROM [29]

The staged injector mounted in the combustor is shown in Figure 2. It comprises: i) a pilot stage with a central injection tube (4 mm in diameter) and the associated radial swirler (geometrical swirl number of 1), and ii) a multipoint stage where the fuel is fed through 15 equally spaced holes (0.7 mm in diameter) in a crossflow of air downstream of a second radial swirler (geometrical swirl number of 0.9) to enable efficient turbulent mixing of fuel and air. The two swirlers are arranged in a co-rotating orientation. To fix ideas, the bulk velocity at the

injector exit is about 16 $m.s^{-1}$ for a 50-kW flame at an equivalence ratio of 0.5.

This Lean Premixed Prevaporized (LPP) injector design provides realistic air-fuel injection and an engine-like recirculation zone in the combustion chamber. The pilot stage creates a fuel-rich region to anchor the flame. The multipoint stage is designed to ensure good mixing of fuel and air to operate in lean premixed conditions. The methane flow rate in each stage is independently controlled to vary the fuel staging factor (Bronkhorst Cori-Flow M55-RAD-44-0-S, Bronkhorst EL-Flow F-203AC-AAD-44-V). The fuel staging factor, α, is defined as the ratio of the fuel mass flow rate injected through the pilot stage to the total fuel mass flow rate:

$$\alpha = \frac{\dot{m}_{CH_4,pilot}}{\dot{m}_{CH_4,multi} + \dot{m}_{CH_4,pilot}} \quad (1)$$

where $\dot{m}_{CH_4,pilot}$ and $\dot{m}_{CH_4,multi}$ are the methane flow rates through the pilot stage and the multipoint stage, respectively. The air flow rate is controlled by a single mass flow controller (Bronkhorst EL-Flow F-206BI-FA-00-V). Air is fed in the plenum and naturally splits, thanks to head losses [13], into a 20-80% distribution between the co-rotating pilot (20%) and multipoint (80%) swirlers. The global equivalence ratio, denoted Φ_g, is defined as the total methane-to-air mass flow rate ratio divided by the stoichiometric methane-to-air mass flow rate ratio.

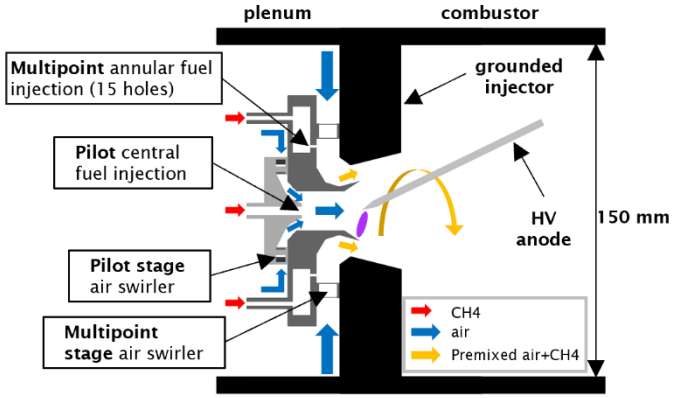

FIGURE 2 CROSS-SECTIONAL VIEW OF THE TWO-STAGE MULTIPOINT INJECTOR WITH THE HIGH-VOLTAGE ELECTRODE ASSEMBLY

As shown in Figure 2, the nanosecond discharges are produced in a pin-to-ring configuration between the high-voltage anode and the rim of the divergent of the pilot stage, which is grounded. The interelectrode gap is approximately 7 mm. The electrode body is water-cooled and made of stainless steel; the tip is made of tungsten. The pulses are applied at a repetition frequency of 33 kHz, with a maximal energy input per pulse of 4 mJ, delivered by a 10-ns-duration high-voltage pulse generator (FID Technology 15-100NM10). The deposited energy is measured using a voltage and a current probes located halfway along the coaxial cable, using the procedure described in Ref. [30]. The reported energy values and their standard deviations are obtained by averaging over about 1000 pulses. Interestingly, we note that for the same applied voltage and pulse repetition frequency, the average deposited energy and the standard deviation may vary significantly depending on the operating conditions (fuel staging, equivalence ratio).

The discharges appear in the form of filaments. Visual observations indicate that the discharges are slightly rotating, but they cover less than half the circle defined by the rim of the divergent of the pilot stage. The NRP discharges in this experiment are either nonequilibrium sparks [12] or thermal sparks [31], further investigations are needed to determine the exact regime.

An ICCD camera (Princeton Instruments, PI-MAX 4) fitted with a 50-mm lens (Nikon, AF Nikkor f/1.4) and a bandpass filter (Asahi spectra, F0101, CWL = 430 nm) centered on the CH* chemiluminescent emission facing one of the silica windows is used for flame imaging. The images presented in this article were recorded with a gate width of 200 µs, integrated along the line of sight, and averaged over 200 samples.

2.2 LBO limit determination

To determine the LBO limit of the burner at constant thermal power P_{flame}, we proceed as follows. First, we ignite a low-power flame, and then we increase the flame power up to the targeted power at an equivalence ratio of 0.8 (or higher if the flame is not stable). To ensure good reproducibility, this operating condition is maintained until the wall surface temperature, controlled with thermocouples, reaches steady state. Then, keeping the methane flow rates constant, the air flow rate is gradually increased to reduce the equivalence ratio until extinction. This procedure is repeated between 5 and 10 times for each operating condition studied. To investigate the influence of the plasma on the lean blow-off, we first determine the limit without plasma and then with NRP discharges. The water-cooled electrode is always present in the chamber, whether the plasma is applied or not.

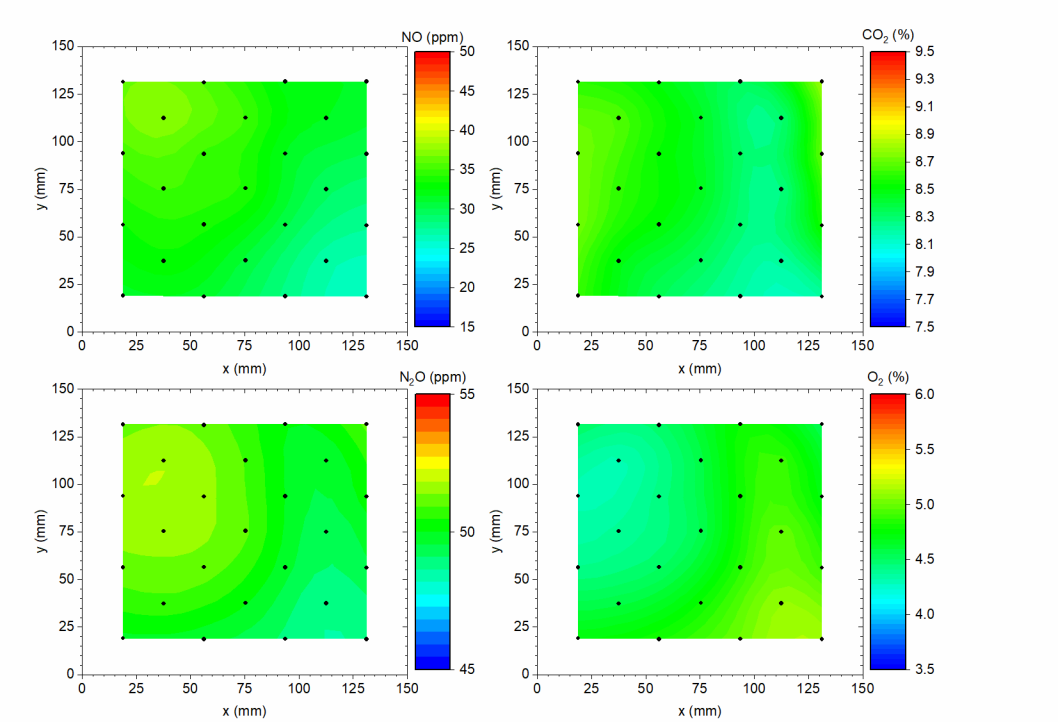

FIGURE 3 NO, CO_2, N_2O AND, O_2 CONCENTRATION FIELDS AT THE CHAMBER OUTLET (RAW DATA) FOR THE FLAME AT 50 kW, $\Phi_g = 0.8$, $\alpha = 100\%$

2.3 Gas analysis

A gas sampling probe is installed at the exit of the chamber and connected to commercial gas analyzers via a heated line to measure the combustion products. A first gas analyzer (SK-electroniks UPAS-FID) comprises a flame ionization detector to measure the total hydrocarbon content (THC), and electrochemical cells for CH_4. A second gas analyzer (Horiba VA-5000) measures CO_2, CO, NO, N_2O based on non-dispersive infrared absorption spectroscopy, O_2 with a paramagnetic cell, and NO_2 with electrochemical cells. To prevent interference from H_2O, water vapor is removed with a cold trap bath from the gas stream before entering the second analyzer. This gas analyzer measures mole fractions in the dried gases. The procedure to infer the actual mole fractions of each species and to deduce the mole fraction of H_2O is presented in Appendix. Note that in Section 3, we present "raw data", i.e. measurements that are not postprocessed. All other data presented in this paper are postprocessed. The combustion efficiency η_c is determined from the gas measurement using the procedure detailed in Appendix.

Gas analysis is carried out as follows during the experiments. Once the flame is set to the chosen operating conditions, we wait for a delay corresponding to the suction of the gas in the sampling line before launching the acquisition. Thanks to the monitoring of the temporal evolution of the measurements, we ensure that the acquisition starts once steady state is reached. Then, measurements are acquired during at least one minute and are temporally averaged. The analyzers were calibrated with commercial bottles of known gas composition matching the scales of the analyzers.

TABLE 1 SPECIES CONCENTRATION AT THE CHAMBER OUTLET WITHOUT PLASMA

50 kW, $\Phi_g = 0.8$, $\alpha = 40\%$							
	CO_2 (%)	CO (ppm)	O_2 (%)	N_2O (ppm)	NO (ppm)	CH_4 (ppm)	THC (ppm)
mean ± std	7.3 ± 0.3	2.5 ± 6.0	7.3 ± 0.5	39.0 ± 2.0	11.9 ± 1.9	0.0 ± 0.0	0.0 ± 0.0
value at the center	7.1	0	7.7	37.6	11.6	0	0
50 kW, $\Phi_g = 0.8$, $\alpha = 100\%$							
	CO_2 (%)	CO (ppm)	O_2 (%)	N_2O (ppm)	NO (ppm)	CH_4 (ppm)	THC (ppm)
mean ± std	8.5 ± 0.2	0.1 ± 0.2	4.4 ± 0.2	50.3 ± 1.0	32.1 ± 3.1	0 ± 0	0 ± 0
value at the center	8.5	0	4.6	51.0	34.0	0	0

3. SPECIES CONCENTRATION FIELDS AT THE CHAMBER OUTLET WITHOUT PLASMA

In this section, we study a 50-kW flame without plasma at an equivalence ratio Φ_g = 0.8 with two fuel staging factors: α = 40% and α = 100%. The gas composition is measured at 25 different locations at the chamber outlet to assess the spatial homogeneity of the gas composition.

Figure 3 shows the concentration fields of NO, CO_2, N_2O, and O_2 at the chamber outlet for the 50-kW flame, Φ_g = 0.8, α = 100%. These 2D plots show that the concentration fields are homogeneous. The same figures were plotted for the other species and for the other flame condition and are similar. To quantify the spatial variation of the measurements, we present in Table 1, for both flame conditions, the average values, the standard deviations of the spatial measurements, and the values at the center of the chambre outlet section for each species. We see that the concentrations are rather homogenous at the chamber outlet with a standard deviation less than 16%. The 0 values refer to values below the detection limit of the analyzers.

Moreover, when comparing the value at the center to the average value, it appears that it always lies within the standard deviation. The burnt gases are thus homogeneously mixed in the extraction plane and in the rest of this work, we will set the gas sampling probe position at the center of the outlet plane and perform a gas measurement only at this position (x = 75 mm, y = 75 mm).

4. RESULTS AND DISCUSSION

In this section, we investigate the lean blow-off limit of a 50-kW flame with and without plasma for different fuel staging factors varying from α = 0% (multipoint-only injection) to α = 100% (pilot-only injection) and we characterize the emissions near blow-off. The NRP discharges are applied at a repetition frequency of 33 kHz with an energy between 2.6 ± 1.2 and 4 ± 0.2 mJ. The average plasma electric power remains below 0.25% of the flame thermal power.

4.1 LBO limit extension with NRP discharges

In Figure 4, the equivalence ratios at blow-off without and with plasma are plotted for fuel staging factors α varying from 0% to 100%. For α greater than 20%, applying the NRP discharges makes it possible to extend the LBO limit by a factor 1.5 to 1.9. We observe that lean flames are stabilized at equivalence ratio between 0.5 and 0.3. Such low values were already obtained in swirl-stabilized combustor but at reduced flame thermal power in Ref. [25]. At α = 0%, the LBO limit is not so significantly extended by the plasma. In that case, only air is fed through the pilot stage and NRP discharges are applied at the exit of the pilot stage injector (see Figure 2). NRP discharges applied in air produce active species such as atomic oxygen [32], [33]. But their short lifetime prevents these species from reaching the flame front. This electrode configuration is then not optimal to stabilize lean flames with multipoint-only fuel injection. For the other flames, i.e. α ≥ 20%, the main difference at extinction between the flame without and with plasma is the flame shape. When the equivalence ratio is reduced without NRP discharges, the flame starts as a stable V-shape flame (Figure 5(a)), and then becomes unstable and rapidly extinguishes. However, when the equivalence is reduced while the NRP discharges are applied, the flame is sustained throughout the unstable region and then stabilizes in a tulip shape, represented in Figure 5(b). The tulip flame is stable. When further reducing the equivalence ratio, the tulip flame gradually attenuates until blow-off. This flame shape transition is observed for all cases at α ≥ 20% (i.e. when part of the methane is injected through the pilot stage).

Similar flame shapes were already observed in swirl-stabilized burners without plasma in Refs [5], [34]. As explained in Ref. [35], the flame shape is related to the flow topology. The V-shape flame is stabilized by a central recirculation zone described by a conical vortex breakdown mode induced by the flame itself, whereas the tulip-shape flame is stabilized by a bubble vortex breakdown mode, naturally present in the nonreactive flow. The change of flame shape is governed by the transition of vortex breakdown mode. The instability responsible for flame extinction without plasma probably corresponds to the transition of the flow topology. This shows that the NRP discharges are able to maintain the flame even when the flow is unstable in the rapid transition phase. In this series of experiments, the tulip-shape flame is never observed without discharges. Moreover, if the NRP discharges are turned off when the flame is in the tulip shape, the flame survives for a few instants (at most one minute) and then always quickly blows off.

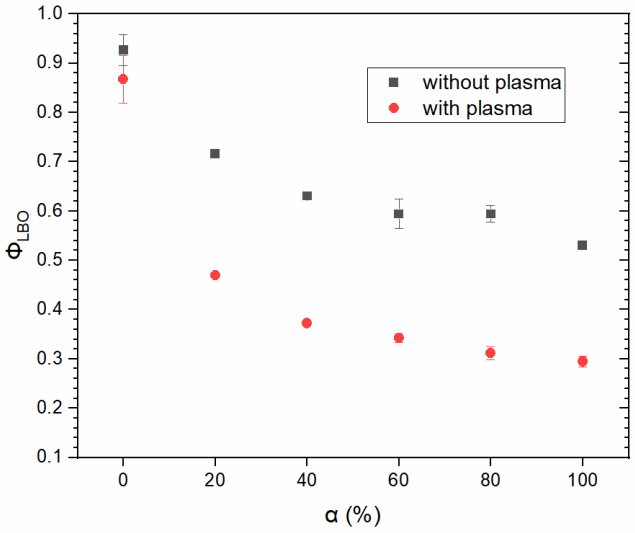

FIGURE 4 LEAN BLOW-OFF LIMIT WITH AND WITHOUT PLASMA OF A 50-kW FLAME VS. FUEL STAGING FACTOR

Flame shape transitions in swirl-stabilized combustors were already observed by Kim *et al.* [17], Choe & Sun [25], and Vignat *et al.* [19]. Applying NRP discharges in a lean flame at steady conditions, Kim *et al.* observed a transition of a flame

stabilized in the outer recirculation zone to a flame stabilized in the central recirculation zone. Choe & Sun found similar results at several flame thermal powers and equivalence ratios. For different flames that were not stabilized over the inner shear layer, they observed that applying NRP discharges begets the flame stabilization over the inner shear layer. Vignat *et al.* decreased the equivalence ratio of liquid n-heptane and dodecane flames. Without plasma, they observed that the flame becomes unstable and extinguishes but applying NRP discharges, they could sustain the flame and stabilize a flame with a shape that does not exist without plasma. The oscillation phase induced by the flame shape transition was responsible for the flame extinction without plasma, as it is the case in the present work.

The benefit of NRP discharges to extend the operation range of this type of injector is hence evidenced. In this work, lean flames are stabilized down to equivalence ratio of 0.3 and also a flame shape, that does not exist otherwise in this configuration, is stabilized.

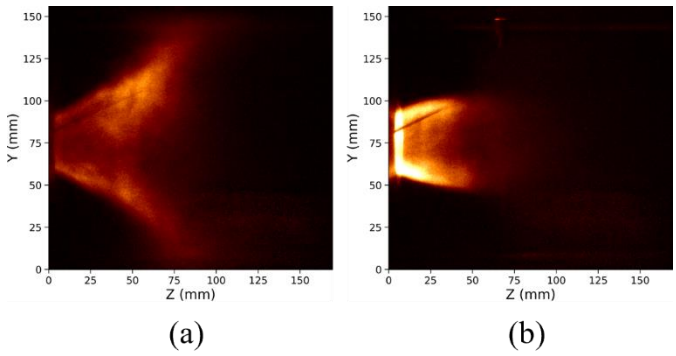

FIGURE 5 CHEMILUMINESCENCE IMAGES OF (a) A V-SHAPE FLAME WITHOUT PLASMA (50 kW, α = 40%, Φ_g = 0.64) AND (b) A TULIP-SHAPE FLAME WITH PLASMA (50 kW, α = 40%, Φ_g = 0.44, E = 3.6 mJ, f = 33 kHz)

4.2 Combustion efficiency and emissions near blow-off

We see in Figure 4, that it is possible to define two equivalence ratios at blow-off for each fuel staging factor. The first one, $\Phi_{LBO,wo}$, corresponds to the equivalence ratio at blow-off without plasma. The second one, $\Phi_{LBO,with}$, is the equivalence ratio at blow-off when NRP discharges are applied. To characterize the emissions near blow-off of these flames, we will operate at equivalence ratios slightly above the equivalence ratios at extinction: 1.1 $\Phi_{LBO,wo}$ and 1.1 $\Phi_{LBO,with}$. At 1.1 $\Phi_{LBO,wo}$ (V-shape flame), we characterize the emissions without plasma but also with plasma to investigate the effect of the NRP discharges on these flames. At 1.1 $\Phi_{LBO,with}$ (tulip-shape flame), as the flame without plasma does not exist, we will characterize the emissions with NRP discharges only. Considering that the chamber length (500 mm) is about 5 times the average length of the tulip-shape flame (see Figure 5), there is enough time for the combustion products to homogenize before reaching the combustor exit plane. Thus, the measurements at the center point should be representative. Further investigations will be performed to confirm this point.

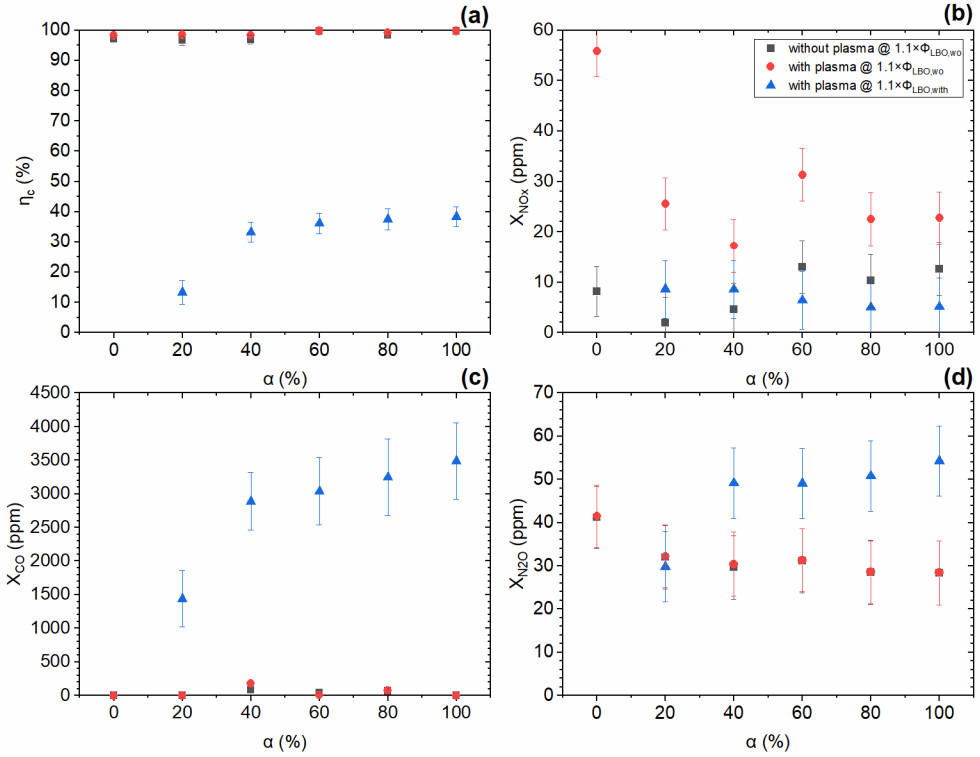

FIGURE 6 COMBUSTION EFFICIENCY (a) AND MOLE FRACTIONS OF NO_X (b), CO (c), AND N_2O (d) NEAR BLOW-OFF AT 50 kW VS. FUEL STAGING FACTORS, WITHOUT PLASMA AT 1.1 $\Phi_{LBO,wo}$ (BLACK SQUARES), WITH PLASMA AT 1.1 $\Phi_{LBO,wo}$ (RED DOTS), AND WITH PLASMA AT 1.1 $\Phi_{LBO,with}$ (BLUE TRIANGLES)

The results for the combustion efficiency η_c, and the mole fractions of NO_X, CO, and N_2O, are shown in Figure 6. For each fuel staging factor, we represent the results at the equivalence ratio 1.1 $\Phi_{LBO,wo}$ without plasma (black squares) and with NRP discharges (red dots) and also at the equivalence ratio 1.1 $\Phi_{LBO,with}$ when NRP discharges are applied (blue triangles). As shown in Figure 6(a), the combustion efficiency of the V-shape flame at 1.1 $\Phi_{LBO,wo}$ without discharges is already above 95% and it increases slightly when NRP discharges are applied. The combustion efficiency of these flames near blow-off is high because during the extinction sequence, as the equivalence ratio was reduced, we do not observe a gradual attenuation of the flame. It means that V-shape flames in this burner have a very satisfying combustion efficiency over the whole range of staging factors. At 1.1 $\Phi_{LBO,with}$, the combustion efficiency of the tulip-shape flame is about 40% for the staging factors between 40% and 100% and falls down to 15% for α = 20%. This lower value compared to the V-shape flame is explained by the change of flame shape and by the visible gradual attenuation of the tulip-shape flame as the equivalence ratio is decreased. However, if we consider that these flames cannot exist without plasma, a combustion efficiency of 40% corresponds to a gain of 19 kW for a plasma power input of only 104 W (3.15 ± 1.00 mJ per discharge at 33 kHz). For α = 0%, we represent only the measurement with and without plasma at the equivalence ratio 1.1 $\Phi_{LBO,wo}$ since $\Phi_{LBO,wo}$ and $\Phi_{LBO,with}$ are very close.

According to the numerical simulations of a comparable two-stage injector [35], the tulip-shape flame exhibits a greater segregation of the flow coming from the two stages in comparison to the V-shape flame. In the tulip-shape, the multipoint-flow poorly mixed with the pilot-flow which fills preferentially the central recirculation zone and thus the reaction zone. In other words, the flow coming from the multipoint stage is probably partially unburnt due to the flow topology that naturally prevents its mixing with the pilot-flow and its penetration in the central recirculation zone. The tulip-shape flame in lean conditions is thus not favorable to a high combustion efficiency and this is accentuated as the fuel staging factor is lowered, i.e. dominated by multipoint fuel injection.

Figure 6(b) shows the NO_X emissions for the three flames. At 1.1 $\Phi_{LBO,wo}$, it appears that the NRP discharges are responsible for an increase of the NO_X emissions for the whole range of fuel staging factors. However, when operating in very lean conditions at 1.1 $\Phi_{LBO,with}$, the level of NO_X emissions is considerably reduced. For α equals 60%, 80%, and 100%, NO_X emissions with NRP discharges are lower than NO_X emissions of the near blow-off flame without plasma (at 1.1 $\Phi_{LBO,wo}$). In Refs. [23], [24], the level of NO_X remains constant as the equivalence ratio of lean flames was decreased with NRP discharges applied. In this work however, the NO_X emissions are reduced when the equivalence ratio of lean flames stabilized by NRP discharges is decreased. This trend is coherent with the work of Lacoste *et al.*

[24] who showed that NO_X emissions linearly increase with the number of pulses per unit mass of air injected in the combustor. In our case, we decrease the equivalence ratio by increasing the air flow rate. Hence, leaner conditions mean higher air flow rate. This work clearly demonstrates that it is possible to stabilize lean flames with NRP discharges, which produce less NO_X than the leanest flames stable without plasma.

Regarding CO and N_2O, the emissions of the V-shape flame at 1.1 $\Phi_{LBO,wo}$ are not altered by the application of NRP discharges for any fuel staging factors, as can be seen in Figure 6(c) and (d). However, the tulip-shape flame with NRP discharges at 1.1 $\Phi_{LBO,with}$ produce a level of CO and N_2O greater than the V-shape flame with NRP discharges for almost all staging factors. The levels of CO and N_2O are higher than those of the V-shape flame with NRP discharges. This can be explained once again by the flow topology. The bubble vortex breakdown mode of the central recirculation zone is responsible for a poor mixing of the flow coming from the two stages. The tulip-shape flame is thus more prone to fuel-rich pockets of gas instead of an efficient fuel-air mixing [35]. This behavior was expected in Ref. [35] to be responsible for higher pollutant emissions and is experimentally confirmed here. We note also that the emissions of CO and N_2O diminish at lower fuel staging factors, as does the combustion efficiency, but this could also be attributed to a better fuel-air mixing as more fuel is fed through the multipoint stage. Finally, as the measurements for the tulip-shape flame are carried out with NRP discharges applied, we cannot distinguish the emissions of the flame itself from the ones due to the plasma.

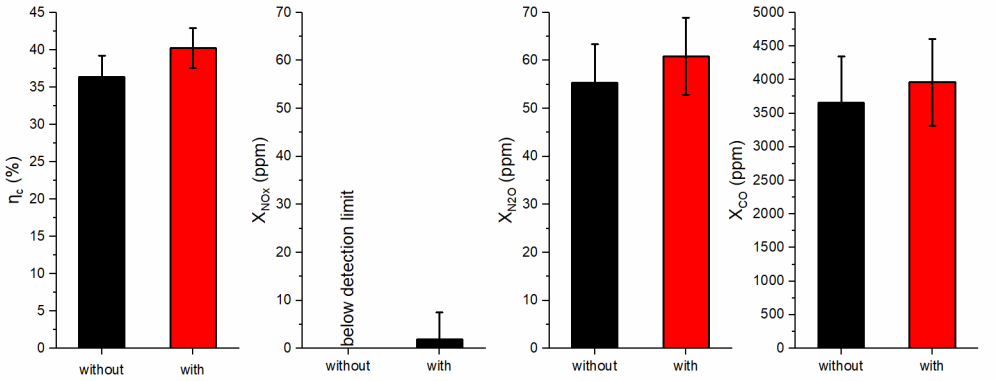

FIGURE 7 COMPARISON OF THE COMBUSTION EFFICIENCY AND EMISSIONS WITHOUT AND WITH NRP DISCHARGES APPLIED AT 33 kHz WITH AN AVERAGE DEPOSITED ENERGY OF 3.4 ± 0.8 mJ OF A 50-kW TULIP-SHAPE FLAME AT α = 80% AND Φg = 0.37

4.3 Tulip shape: impact of NRP discharges

In most cases, if the NRP discharges are turned off when the flame is in the tulip shape, it extinguishes rapidly. However, it was possible to perform a complete cycle of gas analysis for a 50-kW flame at α = 80% and Φ_g = 0.37 without and with NRP discharges. Without the discharges, the flame lives long enough to perform a proper measurement, before being blown off a few instants later. We can thus compare the combustion efficiency and the NO_X, CO, and N_2O emissions of a tulip-shape flame in the same conditions without and with NRP discharges applied at 33 kHz. The results are shown in Figure 7. With NRP discharges, the combustion efficiency of this flame increases from 36% to 40%. The gain in flame thermal power corresponds in this case to 2000 W for a plasma electric power of 113 W. Similar results were obtained by Kim *et al.* [17]. They found that the gain in flame thermal power was 17 times the plasma power. Moreover, we see in Figure 7 that NO_X emissions are below the detection limit without plasma. When NRP discharges are applied, the emissions remain very low, less than 1.8 ppm. At such a low equivalence ratio, the flame is very cold which explains why we cannot detect NO_X without plasma. This means that NO_X are predominantly produced by the plasma. If it is possible to modify the injector design to favor 100% combustion efficiency of these very lean flames stabilized with NRP discharges, then the NO_X emissions would certainly not increase compared to the current flame with a 40% combustion efficiency.

Regarding N_2O emissions, with NRP discharges we measure a few additional ppm, but it appears that this is linked to the improved combustion efficiency. Indeed, we see in Figure 6(a) and (d) that the N_2O emissions of the tulip flames seem proportional to the combustion efficiency. Based on a rough estimate of the linear increase of the N_2O emission with the combustion efficiency, most of the N_2O increase observed in Figure 7 must be due to the improved combustion efficiency when NRP discharges are applied. And finally, without plasma the CO emissions are already high and applying the discharges alters only slightly these emissions.

Based on this comparison, we conclude that the high levels of CO and N_2O emissions of the tulip-shape flame with NRP discharges can be attributed to the flame itself (and its particular tulip topology) rather than to the discharges. The NRP discharges are even beneficial to increase the combustion efficiency.

5. CONCLUSIONS

We have demonstrated in this study that it is possible to stabilize lean flames (down to Φ_g = 0.3) with minimal NO_X emissions (less than 5 ppm) thanks to the application of NRP

discharges in a realistic injector composed of two stages of fuel injection: a pilot stage and a multipoint stage. These results are encouraging. It is the first time to our knowledge that lean hydrocarbon flames stabilized by NRP discharges emit less NO_X than the leanest stable flames without plasma. The operating range of this type of injector is greatly extended thanks to NRP discharges. The plasma-to-flame power ratio remains below 0.25%. The NRP discharges can effectively sustain the combustion and stabilize another type of flame, different from the classical V-shape flame of this burner: the tulip-shape flame. The flame shape is mainly governed by the flow topology and the transition from the V-shape flame to the tulip-shape flame extends the lean blow-off limit compared to the case without plasma. The combustion efficiency of the tulip-shape flame with discharges is about 40% because the flow topology prevents a complete combustion of the fuel injected. The CO and N_2O emissions of the tulip-shape flame with NRP discharges are relatively high in comparison to richer flames stabilized in the V-shape regime. However, these emissions are explained by a detrimental fuel-air mixing induced by this particular flame shape and not by the plasma.

A significant feature of this study is the possibility to stabilize lean flames with a very low level of NO_X emissions in a realistic combustor with NRP discharges. However, if it is performed in already existing burners, it will be complicated to fully benefit from the NRP discharges. Ideally, the injector design should ensure a flow topology that enable the stabilization of lean V-shape flames to minimize the NO_X, CO, and N_2O emissions while maintaining a very high combustion efficiency.

ACKNOWLEDGMENTS

This work was funded by the ANR grant PASTEC ANR16-CE22-0005 and the EU ERC grant GreenBlue ID: 101021538. A CC-BY 4.0 public copyright license has been applied by the authors to the present document and will be applied to all subsequent versions up to the Author Accepted Manuscript arising from this submission, in accordance with the grant's open access conditions: https://creativecommons.org/licenses/by/4.0/. The authors would like to thank Erika Jean-Bart, Yannick Le Teno, Hubert Jubeau, and Koro Sokhona for technical assistance with the experimental facility and Guilhem Lavabre for discussions on uncertainty quantification.

APPENDIX: GAS MEASUREMENTS POSTPROCESSING

The mole fractions of seven species are measured: THC and CH_4 in the combustion products and, CO2, O2, CO, N2O, NO_X in the dried combustion products (where water vapor is removed). Even though NO and NO_2 are measured distinctively from a physical point of view, due to hardware design, both measurements are not decoupled so that we measure either NO only or the sum of NO and NO_2 mole fractions, referred as NO_X in this work. To remain in the range of measurement of the CH_4 and THC analyzers, the gas sampled for these analyzers is diluted by a known factor. In the following calculations, the dilution was accounted for, such that the terms relative to CH_4 and THC appear as undiluted.

To determine the actual mole fractions of the measured species from their mole fractions in the dried gases, we have to infer the H_2O mole fraction from the measurements. We assume that we have the following general reaction between the fresh gases and the combustion products:

$$\begin{aligned}\phi CH_4 + 2(O_2 + 3.76\,N_2) \rightarrow\ & \nu''_{CO_2} CO_2 + \nu''_{H_2O} H_2O + \nu''_{N_2} N_2 \\ & + \nu''_{O_2} O_2 + \nu''_{CO} CO \\ & + \nu''_{CH_4} CH_4 + \nu''_{Y} CH_Y \\ & + \nu''_{NO} NO + \nu''_{NO_2} NO_2 \\ & + \nu''_{N_2O} N_2O\end{aligned} \tag{2}$$

As the exact composition of the THC is not known, we assume only one generic species different from CH_4, CH_Y where Y can take value between 1 and 3. The stoichiometric coefficients are related thanks to atoms conservation:

$$\nu''_{CO_2} = \phi - \nu''_{CO} - \nu''_{CH_4} - \nu''_{Y} \tag{3}$$

$$\nu''_{H_2O} = 2\phi - 2\nu''_{CH_4} - \frac{Y}{2}\nu''_{Y} \tag{4}$$

$$\begin{aligned}\nu''_{O_2} = {} & 2(1-\phi) + \frac{1}{2}\nu''_{CO} + 2\nu''_{CH_4} \\ & + \frac{4+Y}{4}\nu''_{Y} - \frac{1}{2}\nu''_{NO} - \nu''_{NO_2} - \frac{1}{2}\nu''_{N_2O}\end{aligned} \tag{5}$$

$$\nu''_{N_2} = 7.52 - \frac{1}{2}\nu''_{NO} - \frac{1}{2}\nu''_{NO_2} - \nu''_{N_2O} \tag{6}$$

We define the sum of the stoichiometric coefficients with and without the presence of H_2O in the mixture:

$$\begin{aligned}\Sigma\nu''_i - \nu''_{H_2O} = {} & 9.52 - \phi + \frac{1}{2}\nu''_{CO} + 2\nu''_{CH_4} + \frac{4+Y}{4}\nu''_{Y} \\ & - \frac{1}{2}\nu''_{NO_2} - \frac{1}{2}\nu''_{N_2O}\end{aligned} \tag{7}$$

$$\Sigma\nu''_i = 9.52 + \phi + \frac{1}{2}\nu''_{CO} + \frac{4-Y}{4}\nu''_{Y} - \frac{1}{2}\nu''_{NO_2} - \frac{1}{2}\nu''_{N_2O} \tag{8}$$

Finally, the measured mole fraction of each species (superscript m) is related to the stoichiometric coefficients via the following expressions:

$$X^m_{CO_2} = \frac{\phi - \nu''_{CO} - \nu''_{CH_4} - \nu''_{Y}}{\Sigma\nu''_i - \nu''_{H_2O}} \tag{9}$$

$$X^m_{O2} = \frac{2(1-\phi) + \frac{1}{2}\nu''_{CO} + 2\nu''_{CH_4} + \frac{4+Y}{4}\nu''_{Y} - \frac{1}{2}\nu''_{NO} - \nu''_{NO_2} - \frac{1}{2}\nu''_{N_2O}}{\Sigma\nu''_i - \nu''_{H_2O}} \tag{10}$$

$$X^m_{CO} = \frac{\nu''_{CO}}{\Sigma\nu''_i - \nu''_{H_2O}} \tag{11}$$

$$X^m_{CH_4} = \frac{\nu''_{CH_4}}{\Sigma\nu''_i} \quad (12)$$

$$X^m_{CH_Y} = \frac{\nu''_{CH_Y}}{\Sigma\nu''_i} \quad (13)$$

$$X^m_{CH_Y} = X^m_{THC} - X^m_{CH_4} \quad (14)$$

$$X^m_{N_2O} = \frac{\nu''_{N_2O}}{\Sigma\nu''_i - \nu''_{H_2O}} \quad (15)$$

$$X^m_{NO_x} = \frac{\nu''_{NO} + \alpha\nu''_{NO_2}}{\Sigma\nu''_i - \nu''_{H_2O}} \quad (16)$$

where α stands for the NO_2 electrochemical cells efficiency, measured to be 0.774.

Rearranging the different equations, the stoichiometric coefficients are determined by solving:

$$Ax = b \quad (17)$$

where the matrix A is defined as:

$$A = \begin{pmatrix} 1+X^m_{CO_2} & -1-\frac{1}{2}X^m_{CO_2} & -1-2X^m_{CO_2} & -1-\frac{4+Y}{4}X^m_{CO_2} & 0 & \frac{1}{2}X^m_{CO_2} & \frac{1}{2}X^m_{CO_2} \\ -2+X^m_{O_2} & \frac{1}{2}\left(1-X^m_{O_2}\right) & 2\left(1-X^m_{O_2}\right) & \frac{4+Y}{4}\left(1-X^m_{O_2}\right) & -\frac{1}{2} & -1+\frac{1}{2}X^m_{O_2} & -\frac{1}{2}+\frac{1}{2}X^m_{O_2} \\ X^m_{CO} & 1-\frac{1}{2}X^m_{CO} & -2X^m_{CO} & -\frac{4+Y}{4}X^m_{CO} & 0 & \frac{1}{2}X^m_{CO} & \frac{1}{2}X^m_{CO} \\ -X^m_{CH_4} & -\frac{1}{2}X^m_{CH_4} & 1 & -\frac{4-Y}{4}X^m_{CH_4} & 0 & \frac{1}{2}X^m_{CH_4} & \frac{1}{2}X^m_{CH_4} \\ -X^m_{CH_Y} & -\frac{1}{2}X^m_{CH_Y} & 0 & 1-\frac{4-Y}{4}X^m_{CH_Y} & 0 & \frac{1}{2}X^m_{CH_Y} & \frac{1}{2}X^m_{CH_Y} \\ X^m_{NO_X} & -\frac{1}{2}X^m_{NO_X} & -2X^m_{NO_X} & -\frac{4+Y}{4}X^m_{NO_X} & 1 & \alpha+\frac{1}{2}X^m_{NO_X} & \frac{1}{2}X^m_{NO_X} \\ X^m_{N_2O} & -\frac{1}{2}X^m_{N_2O} & -2X^m_{N_2O} & -\frac{4+Y}{4}X^m_{N_2O} & 0 & \frac{1}{2}X^m_{N_2O} & 1+\frac{1}{2}X^m_{N_2O} \end{pmatrix} \quad (18)$$

And b and x are defined by:

$$b = \begin{pmatrix} 9.52X^m_{CO_2} \\ 9.52X^m_{O_2} - 2 \\ 9.52X^m_{CO} \\ 9.52X^m_{CH_4} \\ 9.52X^m_{CH_Y} \\ 9.52X^m_{NO_X} \\ 9.52X^m_{N_2O} \end{pmatrix} \quad (19)$$

$$x = \begin{pmatrix} \phi \\ \nu''_{CO} \\ \nu''_{CH_4} \\ \nu''_{Y} \\ \nu''_{NO} \\ \nu''_{NO_2} \\ \nu''_{N_2O} \end{pmatrix} \quad (20)$$

The x vector is determined by solving the equation Ax = b with a least square algorithm. In this study, we take Y = 1 to process the data.

Once the stoichiometric coefficients are computed, we determine the mole fractions X_s of each species s.

For the species of the dried combustion products (CO_2, O_2, CO, NO, N_2O, and NO_2), if one species is measured with a concentration below 200 ppm, we deduce its mole fraction from:

$$X_s = X^m_s \times \frac{\Sigma\nu''_i - \nu''_{H2O}}{\Sigma\nu''_i} \quad (21)$$

where X^m_s is the measured value in the dried combustion products of species s.

The combustion efficiency for lean mixtures η_c is defined as the ratio of the variation of enthalpies of formation of the incomplete combustion reaction to the variation of enthalpies of formation of the complete reaction.

$$\eta_c = \frac{\phi\bar{h}^0_{CH_4} - \nu''_{CO_2}\bar{h}^0_{CO_2} - \nu''_{H_2O}\bar{h}^0_{H_2O} - \nu''_{CO}\bar{h}^0_{CO} - \nu''_{CH_4}\bar{h}^0_{CH_4} - \nu''_{Y}\bar{h}^0_{CH_Y}}{\phi\bar{h}^0_{CH_4} - \phi\bar{h}^0_{CO_2} - 2\times\phi\bar{h}^0_{H_2O}} \quad (22)$$

The products of incomplete combustion contain CO and unburnt hydrocarbons in the burnt gases whereas the products of complete combustion are only CO_2, O_2, and H_2O. The standard enthalpies of formation at 1 atm and 298.15 K are given in Table 2.

TABLE 2 STANDARD ENTHALPIES OF FORMATION AT 1 ATM AND 298.15 K

Species	Standard enthalpy of formation (kJ/mol)	Reference
$\bar{h}^0_{CH_4}$	-74.48	[36]
$\bar{h}^0_{CO_2}$	-393.30	[36]
$\bar{h}^0_{H_2O}$	-241.84	[36]
$\bar{h}^0_{CO}$	-110.46	[36]
$\bar{h}^0_{CH_3}$	145.69	NIST chemistry webbook
$\bar{h}^0_{CH_2}$	386.39	NIST chemistry webbook
$\bar{h}^0_{CH}$	594.13	NIST chemistry webbook

This procedure enables to deduce the absolute mole fractions X_s of each species s at the combustor exit plane and the combustion efficiency knowing the mole fractions X_s^m of the species s measured in the dried gases (except for CH_4 and THC measured without removing water vapor). The uncertainties on the results (X_s and η_c) thus depend on the uncertainties on the measurements X_s^m.

Two sources of uncertainties are identified: (1) the temporal fluctuations of the measurements (data are acquired during about 1 minute), denoted σ_1 and (2) the instrumental uncertainties, denoted σ_2. The accuracy of each gas analyzer is 0.5% of full scale according to manufacturer specifications. To estimate the uncertainty, we assume a continuous uniform distribution, and we get for the standard deviation:

$$\sigma_2 = \frac{2\times 0.05\times \text{full scale}}{\sqrt{12}} \tag{23}$$

The σ_2 values of each gas analyzer are reported in Table 3. In the end, we neglect σ_1 because it is always negligible relative to σ_2.

TABLE 3 GAS ANALYZERS FULL SCALE AND ESTIMATE OF THE CORRESPONDING UNCERTAINTY ASSUMING A UNIFORM CONTINUOUS LAW

Species	Analyzer full scale	σ_2
N_2O	5000 ppm	14.4 ppm
CO	1000 ppm	2.9 ppm
O_2	100%	0.3%
CO_2	100%	0.3%
NO	2500 ppm	7.2 ppm
CO	20%	0.06%
CH_4	2000 ppm	5.8 ppm
THC	2000 ppm	5.8 ppm

A Monte-Carlo method is used to determine the final values of the mole fractions at the burner exit, the combustion efficiency, and the corresponding uncertainties. We consider that the measurements X_s^m are random variables with a probability density function defined by a continuous uniform distribution over the interval $[X_s^m - \sigma_{2,s}, X_s^m + \sigma_{2,s}]$. We then generate N = 10,000 samples of the input random variables according to their probability distribution (the number of samples is chosen to ensure convergence of the results) and we solve Eq. 17 for each sample i to determine the output variables ($X_{s,i}$ and $\eta_{c,i}$). For each output variable, we consider $\bar{Y}$ the value averaged over the N results and the corresponding uncertainty σ is the square root of the unbiased variance:

$$\bar{Y} = \frac{1}{N}\sum_{i=1}^{N} Y_i \tag{24}$$

$$\sigma = \left(\frac{1}{N-1}\sum_{i=1}^{N}(\bar{Y} - Y_i)^2\right)^{1/2} \tag{25}$$

REFERENCES

[1] European Commission. Directorate-General for Mobility and Transport. Directorate-General for Research and Innovation., *Flightpath 2050 : Europe's vision for aviation : maintaining global leadership and serving society's needs.* 2011.

[2] Y. Huang and V. Yang, "Dynamics and stability of lean-premixed swirl-stabilized combustion," *Prog. Energy Combust. Sci.*, vol. 35, no. 4, pp. 293–364, 2009, doi: 10.1016/j.pecs.2009.01.002.

[3] J. C. Broda, S. Seo, R. J. Santoro, G. Shirhattikar, and V. Yang, "An experimental study of combustion dynamics of a premixed swirl injector," *Symp. Combust.*, vol. 27, no. 2, pp. 1849–1856, Jan. 1998, doi: 10.1016/S0082-0784(98)80027-1.

[4] S. Barbosa, P. Scouflaire, and S. Ducruix, "Time resolved flowfield, flame structure and acoustic characterization of a staged multi-injection burner," *Proc. Combust. Inst.*, vol. 32 II, pp. 2965–2972, 2009, doi: 10.1016/j.proci.2008.06.139.

[5] A. Renaud, S. Ducruix, P. Scouflaire, and L. Zimmer, "Flame shape transition in a swirl stabilised liquid fueled burner," *Proc. Combust. Inst.*, vol. 35, no. 3, pp. 3365–3372, 2015, doi: 10.1016/j.proci.2014.07.012.

[6] J. G. Lee, K. Kim, and D. A. Santavicca, "Effect of injection location on the effectiveness of an active control system using secondary fuel injection," *Proc. Combust. Inst.*, vol. 28, no. 1, pp. 739–746, Jan. 2000, doi: 10.1016/S0082-0784(00)80276-3.

[7] B.-S. Hong, A. Ray, and V. Yang, "Wide-range robust control of combustion instability," *Combust. Flame*, vol. 128, no. 3, pp. 242–258, Feb. 2002, doi: 10.1016/S0010-2180(01)00349-2.

[8] G.-M. Choi, M. Tanahashi, and T. Miyauchi, "Control of oscillating combustion and noise based on local flame structure," *Proc. Combust. Inst.*, vol. 30, no. 2, pp. 1807–1814, Jan. 2005, doi: 10.1016/j.proci.2004.08.249.

[9] S. M. Starikovskaia, "Plasma assisted ignition and combustion," *J. Phys. D. Appl. Phys.*, vol. 39, no. 16, 2006, doi: 10.1088/0022-3727/39/16/R01.

[10] A. Starikovskiy and N. Aleksandrov, "Plasma-assisted

ignition and combustion," *Prog. Energy Combust. Sci.*, vol. 39, no. 1, pp. 61–110, 2013, doi: 10.1016/j.pecs.2012.05.003.

[11] Y. Ju and W. Sun, "Plasma assisted combustion: Dynamics and chemistry," *Prog. Energy Combust. Sci.*, vol. 48, pp. 21–83, 2015, doi: 10.1016/j.pecs.2014.12.002.

[12] D. Z. Pai, D. A. Lacoste, and C. O. Laux, "Nanosecond repetitively pulsed discharges in air at atmospheric pressure-the spark regime," *Plasma Sources Sci. Technol.*, vol. 19, no. 6, p. 065015, 2010, doi: 10.1088/0963-0252/19/6/065015.

[13] S. M. Starikovskaia, "Plasma-assisted ignition and combustion: Nanosecond discharges and development of kinetic mechanisms," *J. Phys. D. Appl. Phys.*, vol. 47, no. 35, 2014, doi: 10.1088/0022-3727/47/35/353001.

[14] C. O. Laux, "Applications of Plasma Discharges to Combustion," *J. Combust. Soc. Japan*, vol. 64, no. 209, pp. 257–264, 2022, doi: 10.20619/jcombsj.64.209_257.

[15] G. Pilla, D. Galley, D. A. Lacoste, F. Lacas, D. Veynante, and C. O. Laux, "Stabilization of a Turbulent Premixed Flame Using a Nanosecond Repetitively Pulsed Plasma," *IEEE Trans. Plasma Sci.*, vol. 34, no. 6, pp. 2471–2477, Dec. 2006, doi: 10.1109/TPS.2006.886081.

[16] J. P. Moeck, D. A. Lacoste, C. O. Laux, and C. O. Paschereit, "Control of combustion dynamics in a swirl-stabilized combustor with nanosecond repetitively pulsed discharges," *51st AIAA Aerosp. Sci. Meet. Incl. New Horizons Forum Aerosp. Expo. 2013*, vol. 2013–0565, 2013, doi: 10.2514/6.2013-565.

[17] W. Kim, J. Snyder, and J. Cohen, "Plasma assisted combustor dynamics control," *Proc. Combust. Inst.*, vol. 35, no. 3, pp. 3479–3486, 2015, doi: 10.1016/j.proci.2014.08.025.

[18] S. Shanbhogue, D. Weibel, F. Gomez del Campo, C. Guerra-Garcia, and A. Ghoniem, "Active Control of Large Amplitude Combustion Oscillations using Nanosecond Repetitively Pulsed Plasmas," in *AIAA SCITECH 2022 Forum*, Jan. 2022, pp. 1–16, doi: 10.2514/6.2022-1450.

[19] G. Vignat *et al.*, "Improvement of lean blow out performance of spray and premixed swirled flames using nanosecond repetitively pulsed discharges," *Proc. Combust. Inst.*, vol. 38, no. 4, pp. 6559–6566, Aug. 2021, doi: 10.1016/j.proci.2020.06.136.

[20] F. Di Sabatino and D. A. Lacoste, "Enhancement of the lean stability and blow-off limits of methane-air swirl flames at elevated pressures by nanosecond repetitively pulsed discharges," *J. Phys. D. Appl. Phys.*, vol. 53, no. 35, p. 355201, Aug. 2020, doi: 10.1088/1361-6463/ab8f54.

[21] S. Barbosa *et al.*, "Influence of nanosecond repetitively pulsed discharges on the stability of a swirled propane/air burner representative of an aeronautical combustor," *Philos. Trans. R. Soc. A Math. Phys. Eng. Sci.*, vol. 373, no. 2048, p. 20140335, Aug. 2015, doi: 10.1098/rsta.2014.0335.

[22] W. Kim, H. Do, M. G. Mungal, and M. A. Cappelli, "Flame stabilization enhancement and NOx production using ultra short repetitively pulsed plasma discharges," *Collect. Tech. Pap. - 44th AIAA Aerosp. Sci. Meet.*, vol. 9, no. January, pp. 6770–6772, 2006.

[23] G. D. Stancu, M. S. Simeni, and C. O. Laux, "Investigations by Mid-IR QCLAS of pollutant emissions in high temperature exhaust gases released from plasma-assisted combustion," in *31st ICPIG, July 14-19, 2013, Granada, Spain*, 2013, no. 6, pp. 8–11.

[24] D. A. Lacoste, J. P. Moeck, C. O. Paschereit, and C. O. Laux, "Effect of Plasma Discharges on Nitric Oxide Emissions in a Premixed Flame," *J. Propuls. Power*, vol. 29, no. 3, pp. 748–751, 2013, doi: 10.2514/1.B34819.

[25] J. Choe and W. Sun, "Blowoff hysteresis, flame morphology and the effect of plasma in a swirling flow," *J. Phys. D. Appl. Phys.*, vol. 51, no. 36, 2018, doi: 10.1088/1361-6463/aad4dc.

[26] Y. Xiong, O. Schulz, C. Bourquard, M. Weilenmann, and N. Noiray, "Plasma enhanced auto-ignition in a sequential combustor," *Proc. Combust. Inst.*, vol. 37, no. 4, pp. 5587–5594, 2019, doi: 10.1016/j.proci.2018.08.031.

[27] S. Barbosa, "Étude Expérimentale De La Dynamique De Combustion D'Un Injecteur Multipoint Étagé De Turbine À Gaz," Ph.D. Thesis, Ecole Centrale Paris, 2008.

[28] T. Providakis, "Etude de la dynamique de flamme swirlée dans un injecteur diphasique multipoints étagé," Ph.D. Thesis, Ecole Centrale Paris, 2013.

[29] A. Renaud, "High-speed diagnostics for the study of flame stabilization and transient behaviour in a swirled burner with variable liquid-fuel distribution," Ph.D. Thesis, Ecole Centrale Paris, 2016.

[30] N. Q. Minesi, V. P. Blanchard, E. Pannier, G. D. Stancu, and C. O. Laux, "Plasma-assisted combustion with nanosecond discharges. I: Discharge effects characterization in the burnt gases of a lean flame," *Plasma Sources Sci. Technol.*, vol. 31, no. 4, p. 045029, Apr. 2022, doi: 10.1088/1361-6595/ac5cd4.

[31] N. Minesi, S. Stepanyan, P. Mariotto, G.-D. Stancu, and C. O. Laux, "Fully ionized nanosecond discharges in air: the thermal spark," *Plasma Sources Sci. Technol.*, vol. 29, no. 8, p. 85003, 2020, doi: 10.1088/1361-6595/ab94d3.

[32] D. L. Rusterholtz, D. A. Lacoste, G. D. Stancu, D. Z. Pai, and C. O. Laux, "Ultrafast heating and oxygen dissociation in atmospheric pressure air by nanosecond repetitively pulsed discharges," *J. Phys. D. Appl. Phys.*, vol. 46, no. 46, p. 464010, Nov. 2013, doi: 10.1088/0022-3727/46/46/464010.

[33] N. A. Popov, "Pulsed nanosecond discharge in air at high specific deposited energy: fast gas heating and active particle production," *Plasma Sources Sci. Technol.*, vol. 25, no. 4, p. 044003, Aug. 2016, doi: 10.1088/0963-

0252/25/4/044003.
[34] L. C. C. Mesquita, A. Vié, L. Zimmer, and S. Ducruix, “Numerical analysis of flame shape bifurcation in a two-stage swirled liquid burner using Large Eddy Simulation,” *Proc. Combust. Inst.*, vol. 38, no. 4, pp. 5971–5978, 2021, doi: 10.1016/j.proci.2020.06.044.
[35] L. Cunha Caldeira Mesquita, “Simulation and analysis of the shape, performance, and stability of flames in a two-stage lean-burn aeronautical combustor,” CentraleSupélec, Université Paris-Saclay, 2021.
[36] C. K. Law, *Combustion Physics*. Cambridge University Press, 2006.